A tokamak reactor based on advanced concepts

R. C. Wolf
Institut für Plasmaphysik, Forschungszentrum Jülich,
EURATOM Assocation/FZJ, Trilateral Euregio Cluster, D-52425 Jülich, Germany

Contents

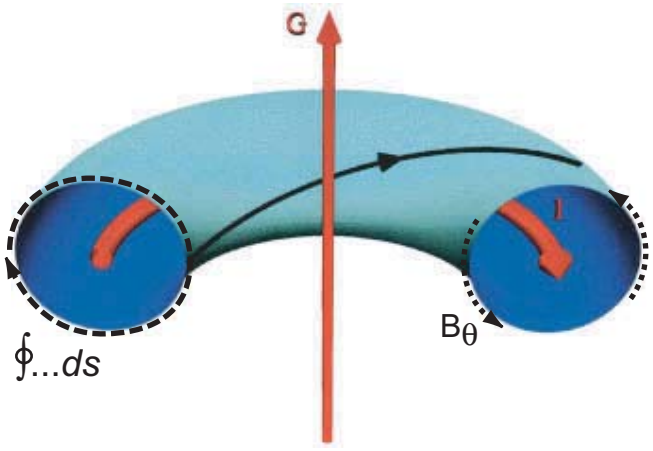

FIG. 1: The tokamak concept (reproduced from [1]). The magnetic field of a tokamak is produced by a toroidal plasma current I in addition to the current G of the toroidal field coils. The primary circuit of the transformer and the vertical field coils, which are needed to balance the hoop stress on the toroidal current, are not shown. The black line is a closed magnetic field line on the q=1 surface.

I. MOTIVATION

A. Magnetic confinement concepts

Based on the fusion reaction between the nuclei of the hydrogen isotopes deuterium and tritium magnetic confinement fusion research aims to develop an electricity producing power plant. The principle concept is to confine a plasma, consisting of these nuclei and their electrons, in a magnetic field configuration in such a way that the thermal plasma can reach temperatures and densities at which sufficient fusion reactions take place to achieve a positive energy balance. The products of the fusion reactions are helium nuclei or α-particles and neutrons. The first, also bound to the magnetic field lines, are supposed to transfer their energy to the thermal plasma and thus sustain the fusion reaction. The latter, because they are not confined by the magnetic field, can leave the plasma directly and are used to breed tritium from lithium and convert the fusion energy into heat.

The two magnetic confinement concepts which have proven successful are the stellarator [1]and the tokamak [2]. Both generate a magneto-hydrodynamic (MHD) equilibrium in a toroidal configuration by superimposing poloidal and toroidal magnetic fields to confine the hot plasma along the magnetic field lines [55].

The tokamak

The basic outline of a tokamak, which operates like a transformer, is depicted in figure 1. The changing current in the primary circuit of the transformer (not shown) induces a toroidal loop voltage which drives the plasma current I. The poloidal magnetic field of I, B_θ, together with the toroidal magnetic field in the direction of the plasma current, produced by the current G, form a helical magnetic field configuration. The helical magnetic field lines follow nested magnetic flux surfaces.

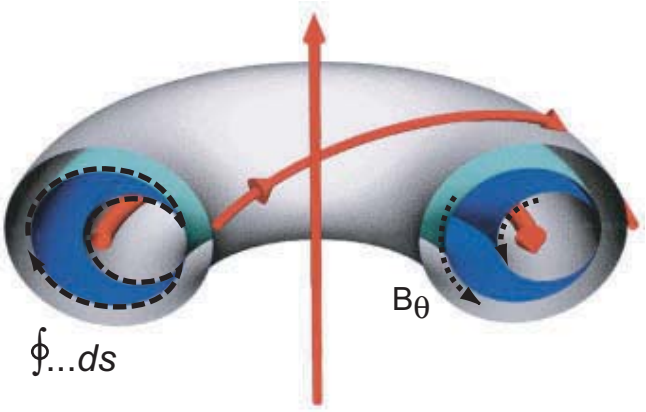

FIG. 2: The stellarator concept (reproduced from [1]). If the configuration of figure 1 is augmented by a helical coil that is parallel to a closed field line on the q =1 surface, a magnetic island is formed. Thus the surface of figure 1 is split to form a magnetic island. The magnetic surfaces inside the island form a stellarator of a type known as a Heliac.

The one indicated in figure 1 by the black line is in so far a special case as it returns to its starting position after exactly one rotation round the torus. This flux surface is therefore also called q =1 surface [56]. As long as the plasma current has to be sustained by the transformer action, the discharge length is limited by the finite flux swing of the transformer. Thus, naturally, a tokamak discharge is pulsed unless means are found to sustain I without the help of the transformer.

The stellarator

A simple version of the stellarator configuration is shown in figure 2. This configuration is generated if the configuration of figure 1 is augmented by a helical coil, which runs parallel to the closed magnetic field line on the q =1 surface, and the plasma current is replaced by coil centered at the same position. As a consequence the flux surface of figure 1 splits to form a magnetic island. The magnetic surfaces inside the island form a special kind of stellarator of a type known as Heliac.

Plasma current and axis-symmetry

In a tokamak the toroidal plasma current enclosed by a magnetic flux surface and the poloidal magnetic field are related via Ampére's law

$$\oint B_\theta ds = \mu_0 I. \qquad (1)$$

On the integration path the poloidal field always points in the same direction (indicated by the dashed and dotted lines in figure 1), which is consistent with an internal plasma current and toroidal axis-symmetry.

By contrast, integrating along a flux surface cross-section in a stellarator, because all currents lie outside the plasma, the poloidal magnetic field changes orientation and hence

$$\oint B_\theta ds = 0. \qquad (2)$$

This also means that toroidal axis-symmetry cannot be retained. In summary, the tokamak configuration is based on an internal plasma current which normally is generated inductively, thus limiting the discharge duration by the finite flux swing of the transformer. A stellarator in contrast is in that respect a configuration which permits steady state operation, but at the expense of loosing the axis-symmetry.

B. Criteria for an advanced tokamak

Classical and neo-classical transport

The basic idea of magnetic confinement is to inhibit the transport of particles and energy perpendicular to the magnetic field, while the charged particles can move close to freely parallel to the magnetic field lines. The basic, minimum transport mechanisms in such plasmas are determined by binary Coulomb collisions. In general this minimum is called "classical". In toroidal configurations, owing to the more complicated particle orbits (trapped particle orbits), this transport is called "neo-classical" [57]. Parallel to the magnetic field neo-classical theory is generally valid. For instance, the parallel electrical conductivity in a tokamak plasma [3],

$$\sigma = \frac{T_e^{3/2}}{f(Z) Z ln\Lambda}, \qquad (3)$$

is in good agreement with experiments [4] (T_e is the electron temperature, $f(Z)$ a weak function of Z, Z the ion charge and $ln\Lambda$ the Coulomb logarithm). However, for the perpendicular or radial transport of energy and particles, neoclassical theory predicts values which are generally too low.

Turbulent transport

While neo-classical theory yields heat conductivities of $\chi_{i,neo} \lesssim 1m^2/s$ for the ions and $\chi_{e,neo} = \sqrt{m_e/m_i}\chi_i$ for the electrons (m_e/m_i is the electron to ion mass ratio), most experiments show $\chi_i \approx \chi_e \approx 10m^2/s$. Also the radial dependence of the heat conductivities does

not agree with neo-classical theory. This discrepancy is attributed to turbulent processes which increase the radial losses, leading to a deterioration of the plasma confinement which is summarized under the term "anomalous" transport [58]. Although theory has made much progress in recent years it is still not possible to describe all aspects of anomalous transport from first principles.

Scaling laws

Therefore the extrapolation to future fusion reactors is based on empirical scaling laws of the energy confinement time, τ_E. A generic example is [5]

$$\tau_E \approx H \frac{I R^2}{\sqrt{P}}. \quad (4)$$

This expression already contains the major ingredients of all scaling laws: The energy confinement increases with plasma current and size of the device (R is the major radius of the torus) and decreases with the square root of the heating power, P. The first might be explained by the trivial point of increased volume to surface ratio. The latter, however, can be understood as a consequence of turbulent processes, which are driven by the free energy of pressure gradients which increase with rising heating power. The factor H describes the confinement quality and differs for different confinement modes: The H factor of the high confinement or H-mode [6], for instance, is typically twice the H factor of the low confinement or L-mode [59].

Fusion power amplification

A measure of the efficiency of the fusion reaction is the power amplification factor, which is defined as the ratio of fusion, P_f, to external heating power, P_h, supplied to the plasma:

$$Q_{DT} = \frac{P_f}{P_h}. \quad (5)$$

Since four times more energy of the fusion reaction is going into the neutrons than into the α-particles and only the α-particles contribute to the self-heating of the plasma,

$$Q_{DT} = \frac{5 P_\alpha}{P_h}. \quad (6)$$

The total heating power, P, is composed of $P = P_h + P_\alpha$. Starting from the power balance of the fusion reaction,

$$P_h + P_\alpha = \frac{W}{\tau_E}, \quad (7)$$

where W is the thermal energy of the plasma and W/τ_E the rate of energy loss from the plasma, a dependence of Q_{DT} on confinement quality, H, toroidal magnetic field, B_ϕ, and major radius of the device, R, can be deduced:

$$Q_{DT} = 5 \left(\frac{const.}{H^2 B_\phi^2 R^3} - 1 \right)^{-1}. \quad (8)$$

Details of the derivation and assumptions made are explained in [7]. In figure 3 the functional dependence of Q_{DT} on (a) major radius and (b) confinement quality is illustrated. Also shown are experimental points of the tokamaks ASDEX Upgrade [8] and JET [9] (the parameters of various tokamak experiments are listed in table I at the end). While the ASDEX Upgrade point is an extrapolation from a pure deuterium plasma, the fusion relevant fuel mixture of deuterium and tritium has been used in JET. In addition, the Q_{DT} range for the planned fusion experiment ITER [10] is indicated, which for the first time shall demonstrate a burning fusion plasma [60].

From equation 8 and figure 3 it is evident that confinement quality, magnetic field strength and size of the tokamak are directly linked. First, it is desirable to make B_ϕ as large as possible. Here, a limit is given by the maximum field which can be attained by super-conducting coils (critical magnetic field) [61]. ITER is already approaching the critical magnetic field. Other restrictions result from technical limitations due to large forces produced by such magnetic fields. The requirement for a large magnetic field is directly related to the plasma current: Assuming a constant safety factor, q_a [62], in the scaling law for τ_E I can be replaced by B_ϕ. Second, increasing the size of the tokamak yields a higher Q_{DT}, which is a result of the "thicker" heat insulation. This possibility, however, has the disadvantage of increased investment costs. Please note, however, that for a reaction a certain volume is required to obtain the desired total fusion power. The third option is the most attractive one, but also the one most difficult to achieve: An improvement of the quality of the heat insulation would increase Q_{DT} without the necessity of a larger device or stronger magnetic field.

A figure of merit for fusion performance

Approaching fully self sustained burning [11] (usually defined as ignition: $Q_{DT} \to \infty$) requires sufficient energy confinement time, τ_E. The ignition condition is often written in form of the tripple product [2],

$$nT\tau_E > 5 \times 10^{21} m^{-3} keV s, \quad (9)$$

which also is inferred from the power balance (equation 7; n, T: plasma density and temperature, respectively). Expressing this in form of β [63] and H, approaching

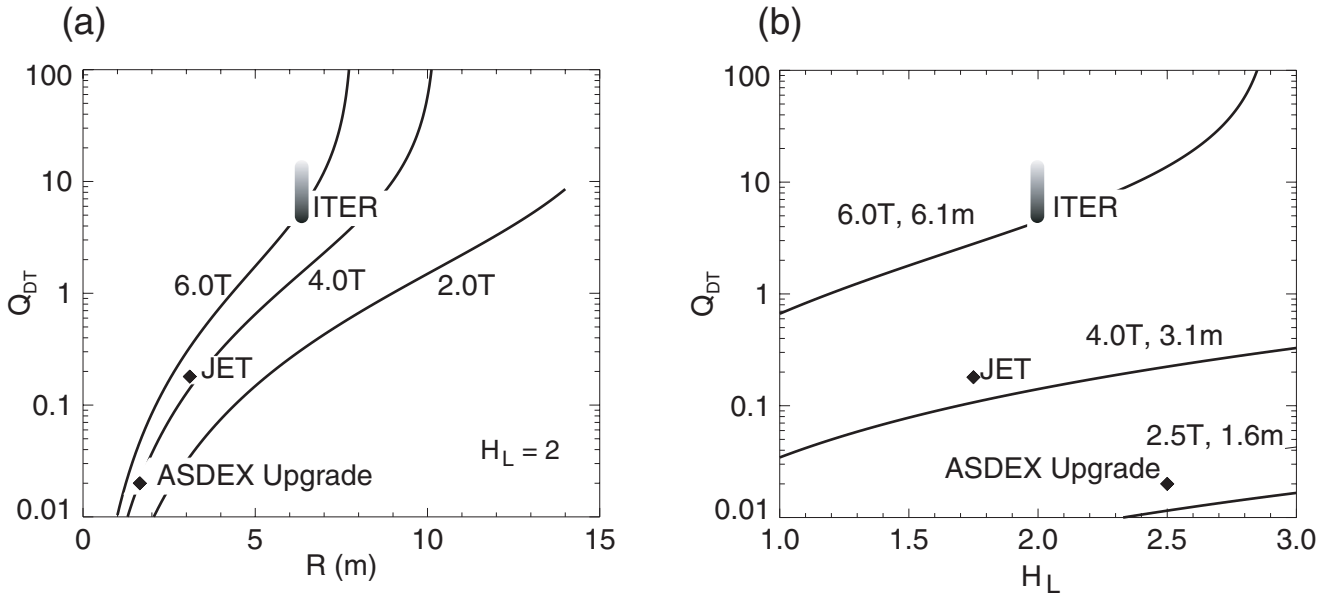

FIG. 3: Dependence of fusion power amplification on (a) major radius of the tokamak and (b) confinement quality [7]. The curves in (a) refer to different toroidal magnetic field strengths of the tokamaks ASDEX Upgrade, JET and ITER. In (b) the curves refer to the respective field strengths and major radii. Here, $H = H_L$ refers to the L-mode, which means that the reference confinement scenario, the H-mode, lies at $H_L \approx 2$.

ignition is tantamount to maximizing $(H/q_a)^2$.

Another optimization criterion is inferred from the requirement of adequate fusion power density, P_f/V, where V is the plasma volume. Considering pressure driven MHD instabilities as the dominant mechanism, limiting the pressure gradient (or average plasma pressure), the fusion power density becomes

$$\frac{P_f}{V} \propto \left(\frac{\beta_N}{q_a}\right)^2. \tag{10}$$

The normalized β,

$$\beta_N = \frac{aB_\phi}{I}\beta(\%), \tag{11}$$

derives from the requirement of stability against so-called ballooning modes [12]. Equation 10 together with maximizing $(H/q_a)^2$ results in a figure of merit for fusion performance, $\beta_N H/q_a^2$, which should be as large as possible (for details see [7]). Basically this means that stability (β_N) and confinement (H) have to be maximized, while keeping q_a and hence the ratio B_ϕ/I as small as possible.

Advanced tokamak concepts

From the previous discussion of confinement and stability, on the one hand, and the need to sustain the plasma current, on the other hand, the aims of advanced tokamak research can be summarized as follows:

- Improving confinement and stability beyond the reference operating scenario for ITER, which is the "standard" H-mode, thus making a future fusion reactor more compact.
- Achieving as far as possible stationary operation by replacing the inductive current by other non-inductive means. As discussed later, these are external current drive by injecting neutral particles or applying electromagnetic waves and the intrinsic bootstrap current which is generated by the pressure gradient of the plasma.

The two aims are inherently linked. A more compact reactor has to operate at lower current which requires improved energy confinement to achieve the same Q_{DT}. On the other hand, a reduction of the plasma current decreases the necessary amount of non-inductive current. Ultimately, the maximum bootstrap current is given by the stability limits determining the achievable pressure gradients.

II. CONFINEMENT MODES

The different confinement modes can be classified into L-mode, H-mode and internal transport barriers (ITBs). The L-mode is governed by a high level of turbulence which is produced by auxiliary heating and enhances the radial transport perpendicular to the magnetic field lines [13]. The combination of sufficiently high heating power and a divertor configuration led to the

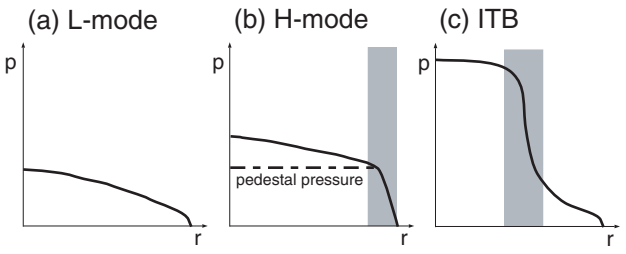

FIG. 4: Illustration of pressure profiles observed in (a) L-mode, (b) H-mode and (c) with an internal transport barrier (ITB). The shaded areas indicate regions of reduced radial transport, which in H-mode is located at the plasma edge and for an ITB in the plasma core.

discovery of the H-mode in the ASDEX tokamak [6]. The H-mode is characterized by a local reduction of the turbulent transport and is associated with an increase of the pressure gradient at the plasma edge. The radial pressure profiles of L- and H-mode are sketched in figure 4(a) and (b). While in L-mode the gradients are limited over the whole plasma cross-section, the H-mode exhibits a region with large gradients at the edge, therefore also termed "edge transport barrier", but a similarly flat region in the plasma core. It is evident from the pressure profile shown that in H-mode the product of pedestal pressure and plasma volume represents already large fractions of the plasma energy. Following the considerations concerning such an edge transport barrier, an internal transport barrier (ITB) may be regarded as a region with a steep pressure gradient inside the plasma, as illustrated in figure 4(c). In order to attain a similar gain of the plasma energy compared to the H-mode, owing to the smaller volume embraced by the internal transport barrier, the pressure increase must be larger accordingly. If the H-mode edge barrier is combined with an internal transport barrier, the contributions of course will add.

A. The H-mode

The "standard" H-mode is one the reference operational scenarios for ITER. Here, "standard" means that the extrapolation of the energy confinement is based on H-mode plasmas, originating from many tokamaks of different sizes, aspect ratios, plasma currents and magnetic fields (other parameters which are contained in the scaling laws are atomic mass of the main plasma species, shaping parameters, such as elongation and triangularity, and plasma density [14]).

Advanced tokamak research aims to extend the range of existing H-mode plasmas towards further improved confinement and stability. The H-mode, however, remains as part of the underlying scenario, being characterized by an edge transport barrier, which is attributed to the local suppression of turbulence.

Turbulent transport and profile stiffness

For understanding H-mode confinement, an essential ingredient is the property of the temperature profiles: They exhibit only little variations of the normalized temperature gradient, R/L_T, in the core region of the plasma, both temporarily and spatially [15–21] (R is the major radius and $L_T = T/|\nabla T|$ the temperature gradient length, where the gradient is taken without sign assuming that it is always negative). How this affects confinement is exemplified in figure 5(a) for ion temperature profiles. Both L- and H-mode exhibit the same gradient length. Owing to the edge transport barrier, however, the edge temperature and thus the plasma energy is much higher in the H-mode. The contribution of the density to the energy is similar in both cases. Internal transport barriers (figure 5(b)), in contrast, can be characterized by values of R/L_{T_i} which significantly exceed those of L- and H-mode plasmas (see later).

The tendency of the temperature profile to stay at a certain value of R/L_T is often called profile resilience or stiffness. This behavior of tokamak plasmas is interpreted as the result of turbulence dominated transport which clamps the normalized gradient at a critical value [22]. Similar to a sand pile, where a certain gradient cannot be exceeded even if more sand is supplied at the top, raising the heat flux causes an increase of the radial energy transport in the plasma once the critical gradient is reached. In other words, the energy transport mechanisms (described by the heat conductivity) adjust themselves to the supply of energy such as to keep R/L_T constant. The weakness of this analogy is that for a sand pile the relevant quantity is the gradient of the number of particles, ∇N, while in a tokamak it is the normalized temperature gradient, R/L_T. Besides, the particle transport in a tokamak does not appear to show such a critical gradient behavior.

So far, the discussion was somewhat simplified, since density gradients, if they are strong enough, can affect R/L_T. In that case not R/L_T, but $\eta = L_n/L_T$ is the relevant quantity which describes the criticality.

Profile stiffness implies that core and boundary temperature are proportional:

$$T(\rho) = T(\rho_b) F(\rho, \rho_b, \varepsilon) \tag{12}$$

$$F(\rho, \rho_b, \varepsilon) = e^{\varepsilon \int_{\rho_b}^{\rho} \alpha(\rho') d\rho'}, \quad \alpha(\rho) = R/L_T, \tag{13}$$

where ρ is the normalized minor radius (e.g. r/a), ρ_b its value at the plasma boundary inside the edge trans-

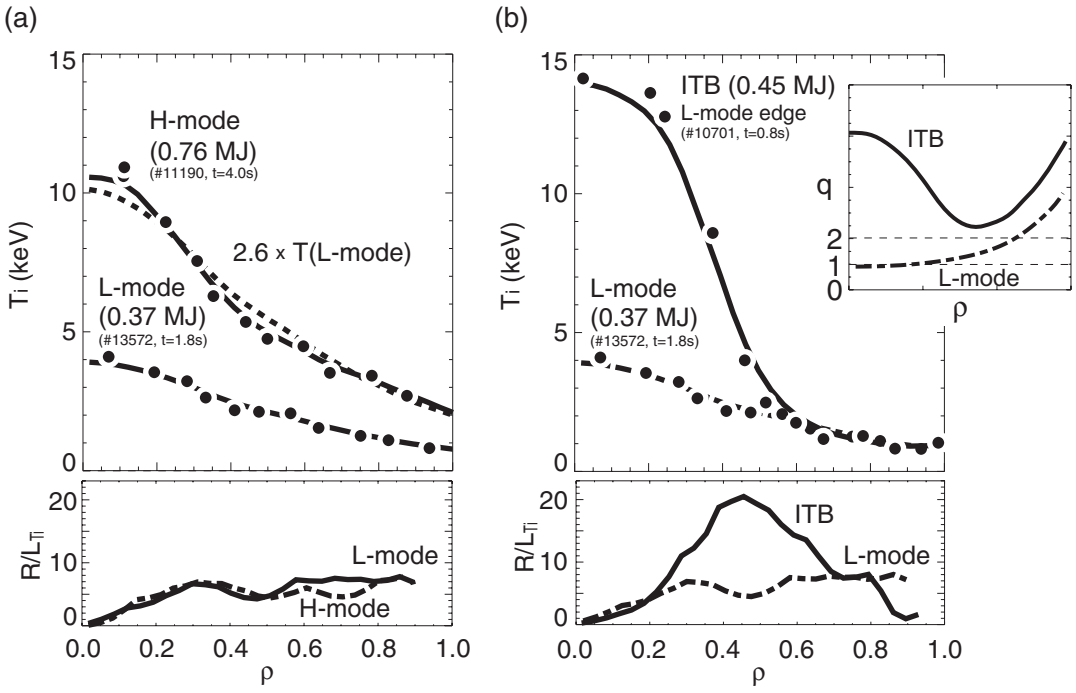

FIG. 5: (a) Ion temperature profiles of L- and H-mode [15]. Both profiles exhibit the same R/L_{T_i}, which is equivalent to profiles which can be mapped onto each other by a constant multiplication factor. Here, the H-mode profile is 2.6 times the L-mode profile (dashed line). (b) In contrast, ITBs show a much larger R/L_{T_i}, produced by modifications of the q profile (see insert).

port barrier, for instance at the H-mode pedestal, and $\varepsilon = a/R$ the inverse aspect ratio. Assuming a radially constant plasma density, $n(\rho) = n(\rho_b)$ and $T_i = T_e$, the plasma energy scales like

$$W \propto \int_0^{\rho_b} nT\rho d\rho = n(\rho_b)T(\rho_b)\int_0^{\rho_b} F(\rho,\rho_b,\varepsilon)\rho d\rho. \quad (14)$$

Thus, for a fixed R/L_T and a given density profile (for simplicity a flat density profile has been chosen in equation (14)) the energy is solely determined by the boundary pressure, $p(\rho_b) = n(\rho_b)T(\rho_b)$, independent of the ratio of density and temperature at the edge. Consequently, an energy increase is equivalent to either an increase of the pedestal pressure or, at constant pedestal pressure, a peaking of the density profile. Regarding the density profile in a burning fusion plasma, a strong peaking seems unlikely, since central fuelling is difficult to achieve and, in H-mode, central heat sources, such as α-particle heating, cause a flattening of the density profile [64]. The latter is explained again by temperature profile stiffness: The reluctance of R/L_T to increase, when the heat flux is raised, is caused by an amplification of the turbulence, which not only increases the heat conduction but also the outward particle flux [23]. From this it follows that the H-mode confinement is essentially determined by the plasma edge properties.

MHD stability

So far, only turbulence driven transport and its effect on confinement have been considered. However, for the energy and particle loss of the plasma MHD instabilities can be equally important, as they determine the achievable plasma β of a tokamak (β-limit) [65]. In the plasma core, such MHD instabilities occur mainly as sawtooth oscillations and neoclassical tearing modes (NTMs) [66]. At the plasma edge, directly associated with the steep pressure gradients of the H-mode edge, they appear in the form of edge localized modes (ELMs) [26], which limit the pressure gradient by expelling energy and particles in form of relaxation oscillations. Not all MHD instabilities are necessary detrimental, as some of them can help to control pressure and impurities in such a way that instabilities, which lead to a termination of the plasma, can be avoided. Other instabilities have to be avoided, such as NTMs, since the confinement degradation they cause is too large. As many of these instabilities depend on the q profile, the tailoring of the q profiles is an essential ingredient of advanced tokamak research to achieve high β-values.

In summary, to improve H-mode confinement and stability above "standard" values, the edge pressure

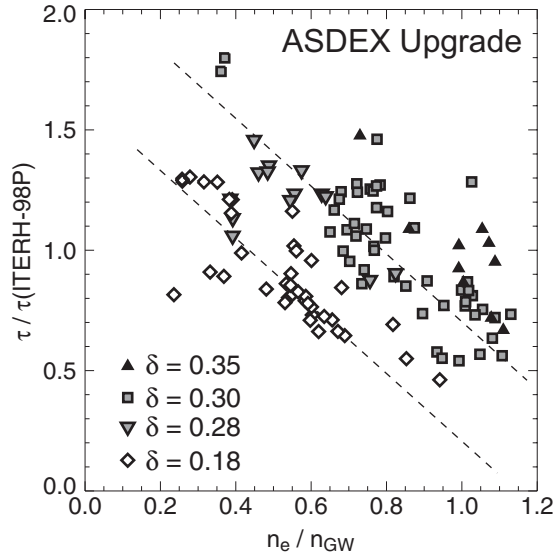

FIG. 6: Confinement time, normalized to H-mode scaling, as a function of the normalized electron density for different values of triangularity, δ, for the tokamak ASDEX Upgrade [24].

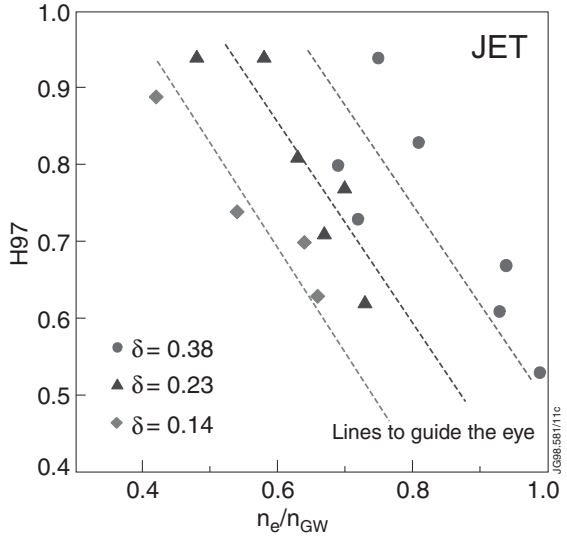

FIG. 7: The same as in figure 6 for the tokamak JET (reproduced from [25]; in linear dimensions JET is about twice the size of ASDEX Upgrade). While the confinement degrades with rising density, it improves with increasing triangularity.

has to be increased (simultaneously avoiding β limiting MHD instabilities).

Plasma shape

Besides the q profile one other essential control parameter is the shape of the plasma cross-section. Historically, tokamak plasmas first had a circular cross-section, later

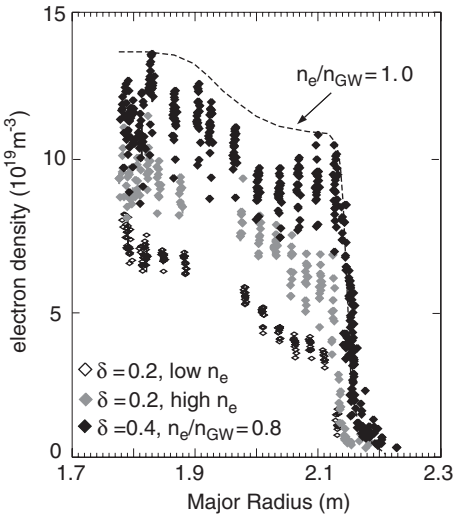

FIG. 8: Electron density profiles for different amounts of gas fuelling rate and triangularity [21]. At low triangularity, $\delta = 0.2$, the density can be raised by increasing the gas flow rate. A much more pronounced increase of the density is achieved by raising the triangularity, $\delta = 0.4$, without additional gas fuelling. The density profile, scaled to the Greenwald density limit, is indicated by the dashed line.

they were vertically elongated to obtain a smaller aspect ratio and more recently it was found that a triangular shape improves H-mode confinement [21, 24, 25, 27]. The effect of triangularity, δ, is shown in figures 6 and 7 for the two tokamaks ASDEX Upgrade and JET, respectively. While for a given δ the confinement degrades with increasing density [67], indicated by the dashed lines, there is an obvious trend towards higher confinement when increasing triangularity.

In agreement with the previous discussion, the main effect of triangularity is improved edge confinement and stability, causing an increase of the pedestal pressure [28]. Consistent with figures 6 and 7 the pedestal pressure increase is mainly carried by a rise of the edge density. This is illustrated in figure 8 which, for ASDEX Upgrade, compares the density profiles for different triangularities. At low triangularity the density can be raised by increasing the gas flow rate at the plasma edge, which however is eventually limited by confinement degradation. A much more pronounced increase of the density is achieved by doubling the triangularity without such degradation.

B. Internal transport barriers (ITBs)

The reduced transport of internal transport barrier plasmas can be characterized by a local exceeding of R/L_T, observed in L- and H-mode plasmas [7, 15, 29]. In figure 5(b) an ion temperature profile with ITB

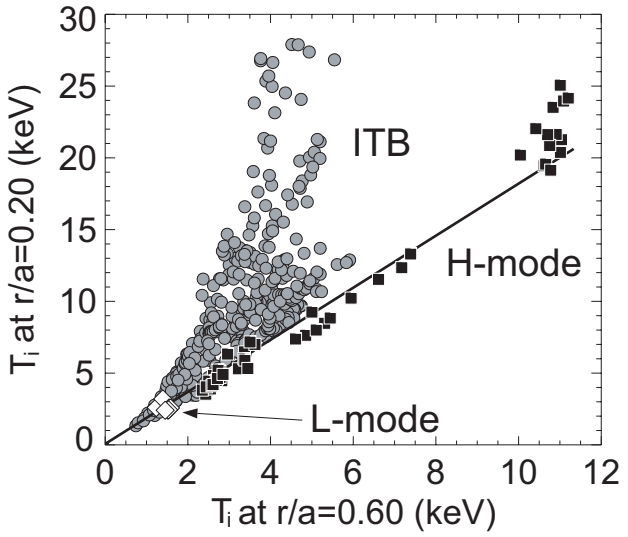

FIG. 9: Central ($\rho = r/a = 0.2$) versus boundary ($\rho_b = r/a = 0.6$) ion temperatures for the tokamak JET [7]. Each point corresponds to one temperature profile. According to equation (12), L- and H-mode profiles show a linear dependence, while ITBs, because of a larger R/L_{T_i}, deviate towards higher central T_i values.

is compared with the L-mode profile of figure 5(a). At about half radius the R/L_{T_i} of the ITB is about three times larger than the corresponding value of the L-mode. Using equation (12), ITBs deviate from the linear dependence towards larger values of $T(\rho)$ for a given $T(\rho_b)$. For JET this is exemplified in figure 9.

Sheared flows and magnetic shear

The two main mechanisms by which ITBs are generated are sheared $\vec{E} \times \vec{B}$ flows and modifications of the magnetic shear [68].

The first depend on the radial electric field which is given by the radial force balance and consists of a $\vec{v} \times \vec{B}$ and pressure gradient term [69]. In short, sheared poloidal and toroidal plasma flows in combination with gradients of the plasma pressure result in a decorrelation of the turbulent eddies which reduces or even suppresses the turbulence responsible for anomalous transport [30]. Due to the presence of magnetic shear, the Kelvin-Helmholtz instability, which grows if sheared flows become too large, seems to be suppressed in tokamak plasmas.

The effects of modifiactions of the magnetic shear (and also the q profile) are twofold, (A) MHD and (B) transport effects.

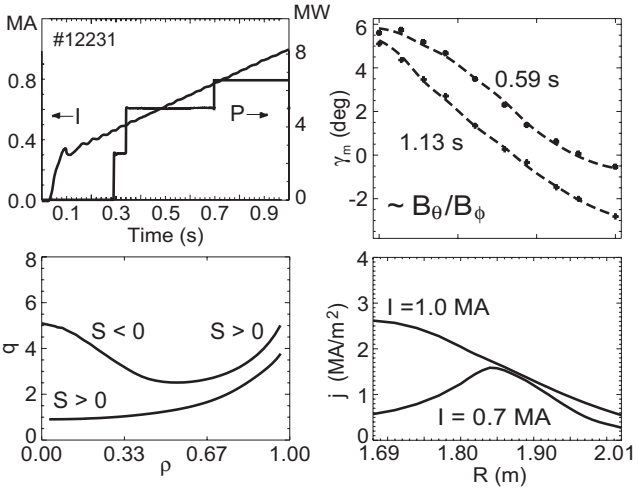

FIG. 10: If during the initial phase of a tokamak discharge, when the plasma current, I, still rises, auxiliary heating power, P, is applied, the current density profile, j, remains hollow and the corresponding q profile non-monotonic for some time (e.g at 0.59s) with regions of negativ, $s < 0$, and positive magnetic shear, $s > 0$. However, without off-axis current drive the current density profile eventually becomes monotonic (at 1.13s). The example shown is an ASDEX Upgrade discharge where the current density profile has been measured using a Motional Stark Effect diagnostic [31, 32]. The measured polarization angle is proportional to the ratio of poloidal to toroidal magnetic field, $\gamma_m \sim B_\theta/B_\phi$.

(A) Certain q values are avoided, which are associated with β limiting MHD instabilities (e.g. $q = 3/2$ for NTMs). In addition, low or negative magnetic shear allows access to the so-called second stability region for ballooning modes, which otherwise would limit the plasma at pressure gradients much lower than those observed in ITB plasmas.

(B) Low or negative magnetic shear, on the other hand, stabilizes many of the turbulent modes which drive the anomalous transport thus making it possible, at least for the ions, to reduce the transport to neoclassical level. Often it is the combination of these effects, i.e. avoidance of MHD instabilities and reduction of turbulence by sheared $\vec{E} \times \vec{B}$ flows and magnetic shear, which causes the formation of internal transport barriers.

Utilizing the skin effect

In a tokamak, q and current density profiles are directly related. Under normal conditions, when the current density profile is allowed to relax completely after discharge initiation, the q profile is monotonic with positive mag-

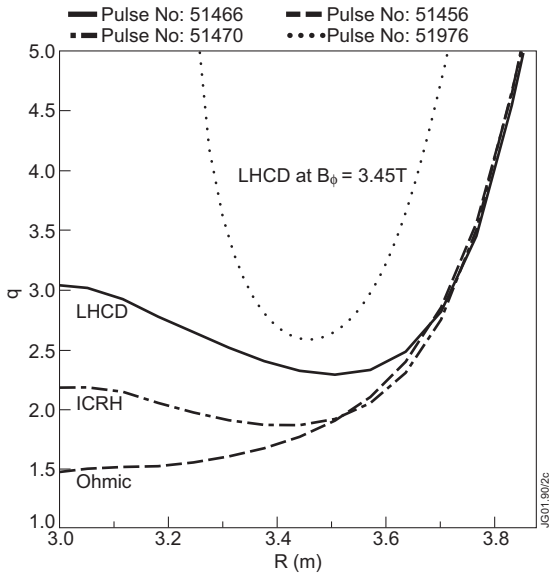

FIG. 11: Overview of q profiles showing the outer half of the plasma obtained in JET using different heating and current drive methods during the current ramp (reproduced from [33]). The heating and current drive systems available at JET are neutral beam injection (NBI), ion cyclotron resonance heating (ICRH) and lower hybrid current drive (LHCD). Ohmic means that except the intrinsic heating by the plasma current no auxiliary heating is applied.

netic shear everywhere and a central q slightly below 1 (see L-mode q profile in figure 5(b)). The most common way to produce negative magnetic shear is to utilize the skin effect: Normally, when initiating the discharge and when the current builds up, the current, initially flowing in the periphery of the plasma due to the skin effect, penetrates rather fast as the plasma is still cold. However, when heating the plasma during this phase, the skin time

$$\tau_{skin} = \mu_0 \sigma a^2 \propto T_e^{3/2} \tag{15}$$

increases and the hollow skin current profile decays on a much longer time scale (the electrical conductivity σ is described by equation (3)). The current density profile corresponds to a non-monotonic q profile with negative magnetic shear in the central regions of the plasma and a minimum q above 1. For an ASDEX Upgrade discharge, the temporal evolution of this process is exemplified in figure 10. The large variety of q profiles which have been achieved at JET with different heating methods during the current ramp are shown in figure 11. Because of the coupling between inductive (or Ohmic) current density and temperature,

$$j_{OH} = \sigma E_\phi, \tag{16}$$

where E_ϕ is the toroidal electrical field induced by the transformer action, a hollow current density profile cannot be sustained by inductive means if the temperature profile is peaked.

Consequently, for maintaining ITBs in a stationary state, all non-monotonic q profiles require an off-axis current source for a sustainment longer than the skin time. The next section discusses the possibility to maintain a stationary plasma current.

III. STATIONARY OPERATION

Requirements for stationary operation

From a fusion reactor point of view the discharge duration, $\tau_{discharge}$, should be as long as possible, preferably many hours. For the characteristic time scales for current diffusion, τ_{skin}, and energy, τ_E, and particle confinement, τ_P, this implies

$$\tau_{discharge} \gg \tau_{skin} > \tau_P \geq \tau_E. \tag{17}$$

The requirements to achieve such stationary operation are manifold:

- To avoid undue thermal losses the coils must be super-conducting, which limits the magnetic field to the critical value for super-conductivity.
- For the plasma facing wall components various processes are of importance. Wall temperature and the gas inventory must reach equilibrium. Ideally a dynamic equilibrium of erosion and re-deposition of wall materials should be reached. This is one of the main issues of ongoing research [70]. Moreover, the neutron damage must not be too large.
- For the toroidal plasma current, stationary operation requires that the inductively generated (Ohmic) part is only used for the initial build-up.

In the following, the last aspect and possible solutions are discussed in detail.

Composition of plasma current

In general, the total (toroidal) current density is composed of Ohmic current, j_{OH}, current driven by external sources, j_{CD}, and bootstrap current, j_{BS}:

$$j = j_{OH} + j_{CD} + j_{BS}. \tag{18}$$

The **Ohmic part** (see equation (16)) is limited in duration by the finite flux swing. Nevertheless, it increases considerably with size. Assuming constant aspect ratio of transformer coils and torus, which contains the plasma, and neglecting the phase of current build-up and decay at the beginning and end of the discharge, the discharge duration scales with the square of the major radius:

$$\tau_{discharge} \propto \frac{q_a}{B_\phi} \sigma R^2 \tag{19}$$

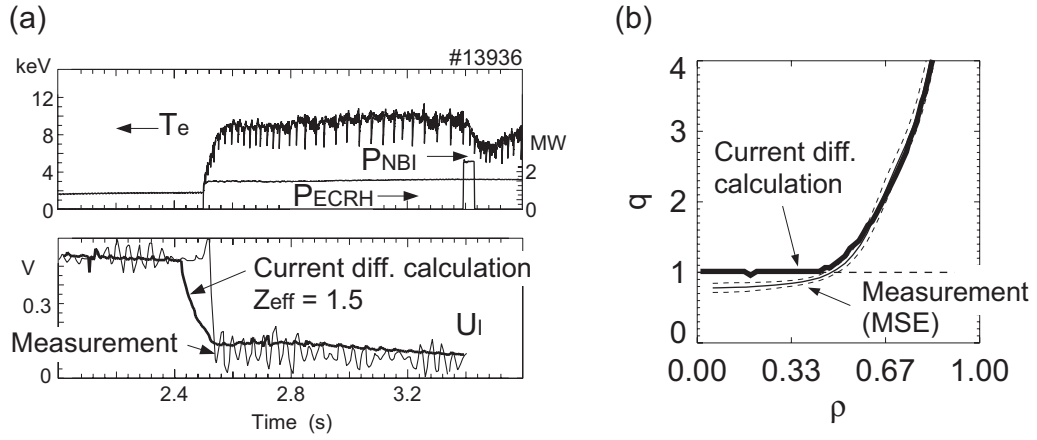

FIG. 12: Effect of electron cyclotron heating and current drive for a low density ASDEX Upgrade discharge [34]. Shown are (a) time traces of ECRH power, P_{ECRH}, neutral beam heating power, P_{NBI}, central electron temperature, T_e, and loop voltage, U_l, and (b) the q profile. The drop of the loop voltage is attributed to an increase of the electrical conductivity and the current driven by ECCD.

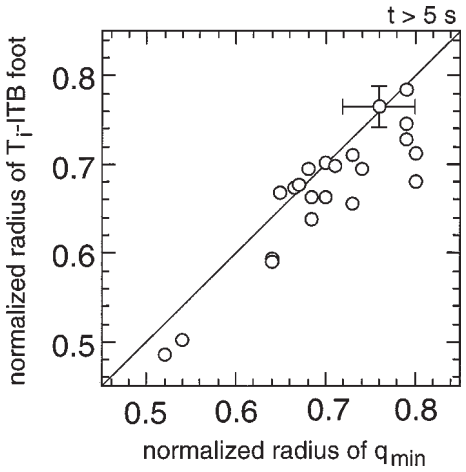

FIG. 13: Relation between location of internal transport barrier and minimum of q profile (reproduced from [35]). A combination of plasma transport and bootstrap current effects contribute to this relation.

External current can be supplied by different **heating and current drive** methods [71] In many cases the heat deposition is closely linked to the current density profile. An example is shown in figure 12. Electron cyclotron resonance heating (ECRH) and current drive (ECCD) is used to support the Ohmic plasma current. The time traces show heating power, central electron temperature and loop voltage. The electron temperature rises considerably when the heating is applied. Because the electrical conductivity rises and current is driven, the loop voltage drops to keep the total plasma current constant, which means that less flux is consumed. The drop of the loop voltage [72] is consistent with a current diffusion calculation, assuming an effective ion charge of Z_{eff} of 1.5. This calculation can also reproduce the measured q profile. Since the external driven current scales like

$$j_{CD} \propto P_h \frac{T_e}{n_e} \propto P_h \frac{p_e}{n_e^2}, \tag{20}$$

the electron density, n_e, is kept low in this discharge to maximize the current drive. In this example the driven current amounts to 82% of the total current. However, at a more fusion relevant electron density of $n_e = 1 \times 10^{20} m^{-3}$ the current drive fraction would drop to a meager 1.6%. Since for fusion relevant particle densities the low efficiency is a general problem of external current drive methods [36], attempts are being made to achieve a high fraction of internal bootstrap current, j_{BS}.

Generally, the **bootstrap current** density is proportional to the pressure gradient:

$$j_{BS} \propto \sqrt{\varepsilon} \frac{\nabla p}{B_\theta} \tag{21}$$

The bootstrap current effect [37–40] is associated with the trapped particles in a tokamak plasma and, therefore, is a consequence of the inhomogeneity of the magnetic field strength, which basically falls of like $1/R$. In contrast to the Ohmic current, which via the electrical conductivity is coupled to the temperature of the plasma, the bootstrap current is linked to the pressure profile which is determined by confinement and stability. As a result, the radius of the ITB is directly related to the radius at which the q profile shows a minimum (see figure 13).

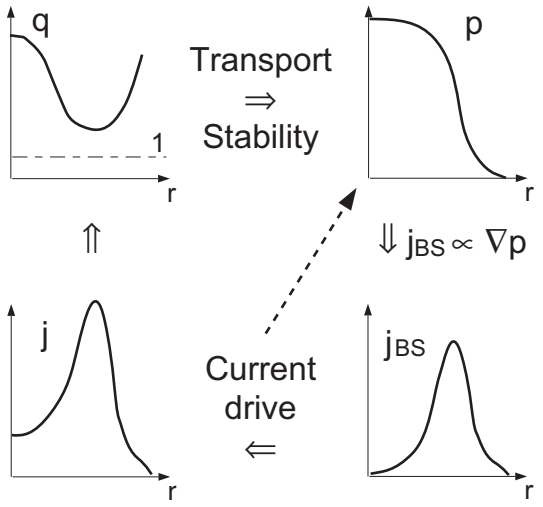

FIG. 14: Consistency between q and pressure profile for full non-inductive current drive ($j_{OH} = \sigma E_\phi = 0$).

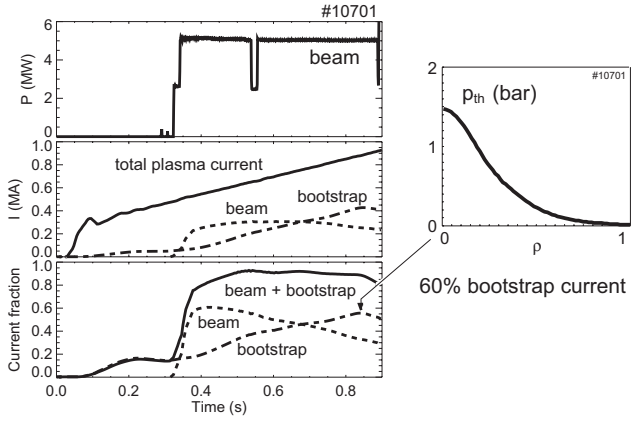

FIG. 15: Temporal evolution of the ASDEX Upgrade ITB plasma shown in figure 5(b). The neutral beam heating, labelled "beam" also provides current drive. Together with the bootstrap current this amounts to nearly 100% of the plasma current. The large bootstrap current fraction of 60% is produced by the strong pressure gradient (p_{th} is the thermal pressure).

Profile consistency

This property of the bootstrap current makes internal transport barrier plasmas with their large internal pressure gradients potentially attractive to achieve stationary tokamak discharges: Summarized under the term "profile consistency", in principle it should be possible to combine pressure and and q profiles, which allow stationary operation without Ohmic current and only little external current drive [40]. The basic idea is sketched in figure 14: Starting from a non-monotonic q profile, transport and stability determine the pressure

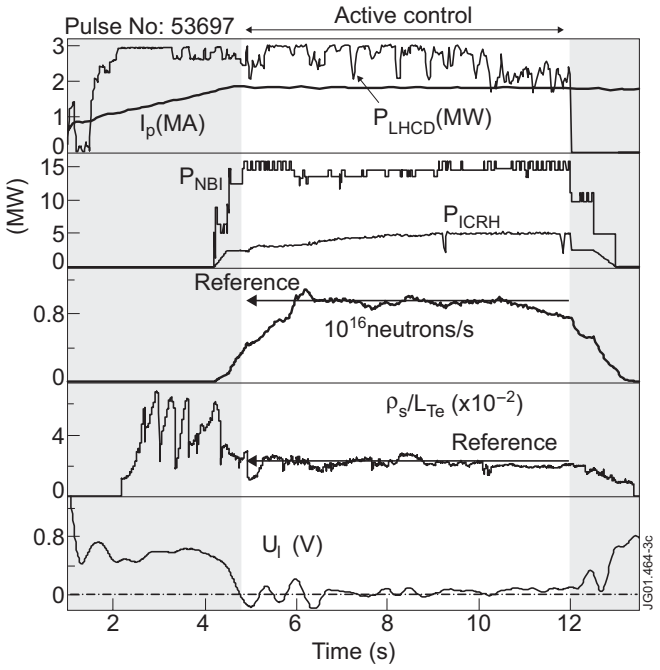

FIG. 16: JET discharge with feedback control of neutron rate and ITB strength, ρ_s/L_{T_e} (reproduced from [41]). The reference values of both are indicated. The neutron rate acts on the NBI power, while the ITB strength is linked to the ICRH power. External current drive is provided by LHCD. The drop of the loop voltage to zero indicates full non-inductive current drive (with about 50% bootstrap current and external current drive fractions, respectively).

profile with the maximum of the pressure gradient (at the ITB location) close to the minimum of the q profile. In the absence of an Ohmic current contribution ($j_{OH} = \sigma E_\phi = 0$) the bootstrap current profile only needs to be modified slightly by external current drive to match the q profile, required to generate the pressure profile. Thus, also the current drive fraction remains low. As current drive methods also heat the plasma, the current drive also acts directly on the pressure profile (indicated by the dashed arrow).

Discharges with high bootstrap current fraction

In figure 15 the temporal evolution of the ITB plasma of figure 5(b) is presented. The discharge reaches almost 100% of non-inductive current drive (i.e. $j_{OH} \to 0$), combining 60% bootstrap and 30% neutral beam current. Similar examples exist for all larger tokamaks [42, 43]. However, despite the large fraction of non-inductive current, up to now many of these discharges last not very long, because current density and pressure profiles with such strong gradients are difficult to control. Often ideal MHD instabilities develop, which are caused by strong pressure gradients in the vicinity of regions with

zero magnetic shear [44].

To avoid these undesired effects it is important to limit the pressure gradient at values within the stability margins. For JET this has been achieved by the feedback control of the neutron production rate and the ITB strength, as illustrated in figure 16 [41]. The loop voltage, which drops to zero, indicates full non-inductive current drive. Although the external current drive fraction is still rather high ($\approx$ 50%), pressure and q profiles are already close to "profile consistency".

IV. SUMMARY AND CONCLUSIONS

Considerable progress has been made in recent years to improve tokamak performance. Values of $Q_{DT}^{eq} = 1$ [73] have been reached or even slightly exceeded in JET [45] and JT-60U [46, 47], although only transiently. In JET these plasmas were based on the ELM free H-modes with high pedestal ion temperatures. As consequence the central ion temperatures reached values, even in the presence of stiff temperature profiles, of up to 25 keV. In JT-60U the high values of Q_{DT}^{eq} were achieved with ITB plasmas. However, in both cases the maximization of the confinement, in JET at the edge and in JT-60U in the core of the plasma, results in insufficient control of pressure gradients and impurity content, eventually leading to the termination of the discharges. Therefore, a compromise between confinement, stability and impurity control has to be found. For comparison, in JET the Q_{DT} of ELMy H-mode plasmas lies at values of 0.2 [9], which are stationary except for the flux consumption required to sustain the plasma current (also excluding plasma wall interaction processes).

Figure 17 summarizes the achievements in terms of the figure of merit, $\beta_N \times H_{89P}$ [74], for a number of different tokamaks [48] (corresponding figures for DIII-D and ASDEX Upgrade alone can be found in [27] and [21], respectively). The figure includes H-mode plasmas, plasmas with ITBs and a combination of both. Also indicated are the reference values for various advanced tokamak studies (ARIES-AT, ITER-AT and SSTR) and the ITER reference scenario (ITER). For shorter durations of the high performance phases, $\tau_{duration}/\tau_E$, rather high values of $\beta_N \times H_{89P}$ have been reached already, even exceeding the reference values of the advanced tokamak scenarios. However, it is also evident that it becomes increasingly difficult to sustain such large values for longer lasting discharges. The JET discharge, shown in figure 16, is such example (in figure 17 labelled "Steady-State with ITB"): The discharge is basically stationary, even with respect to the sustainment of the current profile, but at the expense of a rather moderate $\beta_N \times H_{89P}$. Reasons for this are, that at high β MHD instabilities are difficult to avoid, and,

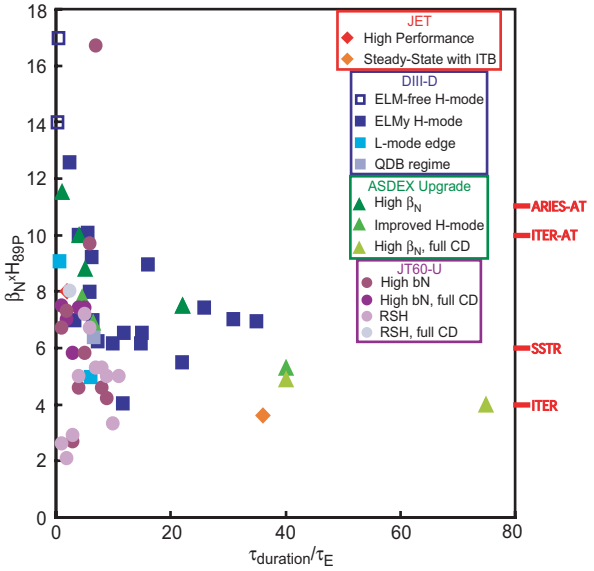

FIG. 17: $\beta_N \times H_{89P}$ for a number of different tokamaks versus normalized duration of high performance phase, $\tau_{duration}/\tau_E$ [48]. H_{89P} refers to an L-mode scaling, meaning $H_{89P} \approx 2$ for a "standard" H-mode. The labels on the right hand side refer to various advanced tokamak studies (ARIES-AT, ITER-AT and SSTR) and the ITER reference scenario (ITER).

that at high confinement plasma pressure and impurity content are difficult to control.

Owing to stronger shaping, in particular increasing the triangularity, H-mode operation has been extended towards higher densities. As ITER reference scenario the H-mode fulfills all major requirements for pulsed operation ($\tau_{discharge} \approx$ 8 minutes). Critical issues which remain are the ELM activity, for which the heat load reaching the divertor target plates may be too large, and NTMs, which would lead to an unacceptable confinement degradation. For both problems various possible solutions are investigated [21, 49–52]. Some of the approaches also include modification of the current density profile to avoid sawtooth oscillations [21, 28] or NTMs [27] by staying above the q values, which are associated with the respective instabilities.

For stationary operation ITB plasmas seem most attractive, because of the potential consistency between pressure and q profile. The possibility of full non-inductive current drive with bootstrap current fractions of up to 80% has been proven [43]. However, the critical issues are whether a compromise between strong internal barriers and a high bootstrap current fraction, on the one hand, and sufficient pressure and impurity control, on the hand, can be found. Approaches include sophisticated feedback control mechanisms, which control pressure gradients and current profile, to stay within the

Device (Institution)	R (m)	a (m)	κ	B_ϕ (T)	I (MA)	Configuration
Alcator C-Mod (MIT, USA)	0.67	0.22	1.7	8.1	1.5	Poloidal Divertor
ASDEX Upgrade (IPP, Germany)	1.65	0.50	1.6	3.9	1.2	Poloidal Divertor
COMPASS-D (UKAEA, UK)	0.56	0.23	1.7	2.1	0.3	Poloidal Divertor
DIII-D (GA, USA)	1.67	0.67	$\leq$2	2.1	1.6	Poloidal Divertor
FT-U (ENEA, Italy)	0.93	0.30	1.0	8.0	1.3	Limiter
JET (Euratom, EU)	3.1	1.25	1.6	4.0	5.0 (7.0)	Poloidal Divertor
ITER (EU, Japan, Russia, USA, China, South Korea)	6.2	2.0	1.7	5.3	15	Poloidal Divertor
JT-60U (JAERI, Japan)	3.4	1.1	<1.8	4.2	2.5	Poloidal Divertor
MAST (UKAEA, UK)	1.0	0.5	2.0	<0.6	<2	Poloidal Divertor
TEXTOR (FZJ, Germany)	1.75	0.46	1	3.0	0.6	Limiter (Dynamic ergodic divertor)
T-10 (Kurchatov, Russia)	1.5	0.37	1	4.5	0.7	Poloidal Limiter
TCV (CRPP, Switzerland)	0.88	0.24	2.6	1.4	1.0	Poloidal Limiter
Tore Supra (CEA, France)	2.37	0.80	1	4.5	2.0	Limiter (Ergodic divertor)

TABLE I: List of parameters of various larger tokamak experiments, which presently are in operation (R: major radius, a: minor radius, κ: elongation, B_ϕ: toroidal magnetic field, I: plasma current). Also listed are the values for the planned experiment ITER [10], which in linear dimensions is about twice as large as JET, which is the largest tokamak to date.

stability margins [41, 53].

In summary, advanced tokamak concepts can be defined by their performance exceeding the ITER reference scenario and, possibly, approaching stationary operation. High performance and stationarity often appear to exclude each other. The task is to find modes of operation, which combine both in an optimal way.

[1] A. H. Boozer, Phys. Plasmas **5**, 1647 (1998).
[2] J. Wesson, *Tokamaks* (Clarendon Press, Oxford, 1997), 2nd ed.
[3] S. P. Hirshman and D. J. Sigmar, Nucl. Fusion **21**, 1079 (1981).
[4] S. H. Batha et al., Phys. Plasmas **4**, 3614 (1997).
[5] R. J. Goldston, Plasma Phys. Control. Fusion **26**, 87 (1984).
[6] F. Wagner et al., Phys. Rev. Lett. **49**, 1408 (1982).
[7] R. C. Wolf, Plasma Phys. Control. Fusion **45**, R1 (2003).
[8] O. Gruber et al., Nucl. Fusion **39**, 1321 (1999).
[9] A. Gibson et al., Phys. Plasmas **5**, 1839 (1998).
[10] D. J. Campbell, Phys. Plasmas **8**, 2041 (2001).
[11] G. H. Wolf, Phys. Bl. **54**, 1109 (1998).
[12] F. Troyon et al., Plasma Phys. Control. Fusion **26**, 209 (1984).
[13] P. N. Yushmanov et al., Nucl. Fusion **30**, 1999 (1990).
[14] ITER Confinement Database and Modelling Working Group, Plasma Phys. Control. Fusion **39**, B115 (1997).
[15] R. C. Wolf et al., accepted for publication in Plasma Phys. Control. Fusion **45** (2003).
[16] R. J. Goldston et al., in *Proc. 11th IAEA Conf. on Plasma Phys. and Nucl. Fusion Research Kyoto (1986), Vol. 1* (IAEA, 1987), p. 75.
[17] R. J. Taylor, M. L. Brown, B. D. Fried, H. Grote, J. R. Liberati, G. J. Morales, P. Pribyl, D. Darrow, and M. Ono, Phys. Rev. Lett. **63**, 2365 (1989).
[18] D. R. Baker, C. M. Greenfield, et al., Phys. Plasmas **8**, 4128 (2001).
[19] G. T. Hoang et al., Phys. Rev. Lett. **87**, 120001 (2001).
[20] F. Ryter et al., Phys. Rev. Lett. **86**, 2325 (2001).
[21] A. C. C. Sips et al., Plasma Phys. Control. Fusion **44**,

B69 (2002).
[22] A. M. Dimits et al., Phys. Plasmas **7**, 969 (2000).
[23] J. Stober et al., Plasma Phys. Control. Fusion **44**, A159 (2002).
[24] J. Stober et al., Plasma Phys. Control. Fusion **42**, A211 (2000).
[25] G. Saibene, L. D. Horton, R. Sartori, et al., Nucl. Fusion **39**, 1133 (1999).
[26] H. Zohm, Plasma Phys. Control. Fusion p. 105 (1996).
[27] T. C. Luce et al., Nucl. Fusion **41**, 1585 (2001).
[28] R. C. Wolf et al., Plasma Phys. Control. Fusion **41**, B93 (1999).
[29] A. G. Peeters et al., Nucl. Fusion **42** (2002).
[30] K. H. Burrell, Phys. Plasmas **4**, 1499 (1997).
[31] F. M. Levinton et al., Phys. Rev. Lett. **63**, 2060 (1989).
[32] R. C. Wolf et al., in *Proc. 24th Eur. Conf. on Controlled Fusion and Plasma Physics, Berchtesgaden* (European Physical Society, Geneva, 1997), p. 1509.
[33] T. J. J. Tala, V. V. Parail, et al., Plasma Phys. Control. Fusion **44**, 1181 (2002).
[34] R. C. Wolf et al., Nucl. Fusion **41**, 1259 (2001).
[35] T. Fujita et al., Nucl. Fusion **38**, 207 (1998).
[36] C. Gormezano, Plasma Phys. Control. Fusion **35**, A239 (1993).
[37] A. A. Galeev and R. Z. Sagdeev, Sov. Phys. JETP **26**, 233 (1968).
[38] R. J. Bickerton, J. W. Connor, and J. B. Taylor, Nat. Phys. Sci. **239**, 110 (1971).
[39] M. Kikuchi and M. Azumi, Plasma Phys. Control. Fusion **37**, 1215 (1995).
[40] A. G. Peeters, Plasma Phys. Control. Fusion **42**, B231 (2000).
[41] D. Mazon et al., Plasma Phys. Control. Fusion **44**, 1087 (2002).
[42] A. Becoulet et al., Plasma Phys. Control. Fusion **43**, A395 (2001).
[43] T. Fujita et al., Phys. Rev. Lett. **87**, 085001 (2001).
[44] J. Manickam et al., in *Proc. 16th IAEA Conf. on Plasma Phys. and Nucl. Fusion Research Montreal (1996), Vol. 1* (IAEA, 1997), p. 453.
[45] JET Team, Nucl. Fusion **32**, 187 (1992).
[46] S. Ishida et al., Phys. Rev. Lett. **79**, 3917 (1997).
[47] T. Fujita et al., Nucl. Fusion **39**, 1627 (1999).
[48] D. J. Campbell, Private communication (2003).
[49] G. Gantenbein et al., Phys. Rev. Lett. **85**, 1242 (2000).
[50] C. M. Greenfield et al., Phys. Rev. Lett. **86**, 4544 (2001).
[51] S. Günter et al., Phys. Rev. Lett. **87**, 275001 (2001).
[52] O. Sauter et al., Phys. Rev. Lett. **88**, 105001 (2002).
[53] G. T. A. Huysmans, T. C. Hender, et al., Nucl. Fusion **39**, 1489 (1999).
[54] M. Greenwald et al., Nucl. Fusion **28**, 2199 (1988).
[55] For details see chapter **EI** in these lectures.
[56] In general the safety factor q describes the helicity of the magnetic field lines and is defined as $q = \frac{\Delta\phi}{2\pi}$, where $\Delta\phi$ is the toroidal angle after which a magnetic field line returns to the same position in the poloidal plane from where it started. For stellarators instead of q normally the rotational transform $\iota = \frac{1}{q}$ is used. The name safety factor refers to the key role which q plays for the MHD stability of the plasma. In a tokamak the q profile is directly related to the profile of the current density
[57] For more information see chapter **TT** in these lectures.
[58] For more information see chapter **AT** in these lectures.
[59] For more details about scaling laws see chapter **SF** in these lectures.
[60] Qualitatively, a fusion plasma can be considered as burning, if the α-power is sufficiently large, e.g $P_\alpha \geq P_h$ or $Q_{DT} \geq 5$. Ignition is equivalent to $Q_{DT} \rightarrow \infty$.
[61] The magnetic field exerts a magnetic pressure, $\frac{B^2}{2\mu_0}$, acting against the pressure gradient of the plasma.
[62] In a tokamak the safety factor close to the plasma boundary is $q_a = f(\text{shape, aspect ratio})\frac{a^2 B_\phi}{RI}$, where a is the minor radius of the plasma at the boundary.
[63] The normalized pressure, $\beta = \frac{p}{B^2/(2\mu_0)}$, represents the efficiency of confinement of plasma pressure by the magnetic field (for more details see chapter **EI** in these lectures).
[64] An exception, causing a density peaking, may be an anomalous particle pinch due to trapped electron modes.
[65] See also chapter **EI** in these lectures.
[66] For a detailed description of these MHD instabilities see chapter **EI-5** and **EI-6** in these lectures
[67] Here, the density is normalized to the Greenwald density, which is an empirically observed density limit, scaling like $n_{GW} \propto I/(\pi a^2)$ [54].
[68] The magnetic shear is the normalized spatial derivative of the q profile: $s = \frac{r}{q}\frac{dq}{dr}$.
[69] For details see chapter **AT-3** in these lectures.
[70] See chapters **EE-2 and EE-3** in these lectures.
[71] For details see chapter **HC** in these lectures.
[72] Loop voltage, U_l, and toroidal electric field are related by $E_\phi = \frac{U_l}{2\pi R}$. For a fully relaxed (equilibrated) current profile, i.e. no current diffusion takes place, the loop voltage is spatially constant. In this case the loop voltage, measured on the plasma surface is the same also inside the plasma.
[73] Q_{DT}^{eq} is the Q_{DT} value extrapolated from pure deuterium plasma to plasma with the fusion relevant mixture of deuterium and tritium.
[74] In this illustration, q_a is not considered. For some of the points, which correspond to a higher q_a, this would mean a lower value of $\beta_N \times H_{89P}/q_a^2$, if q_a was included.